coatings

MDPI

Article

Gas Sensitivity of IBSD Deposited TiO_2 Thin Films

Aleksei V. Almaev [1,2,*], Nikita N. Yakovlev [1], Bogdan O. Kushnarev [1], Viktor V. Kopyev [1], Vadim A. Novikov [1], Mikhail M. Zinoviev [1,3,4], Nikolay N. Yudin [1,3,4], Sergey N. Podzivalov [1,3], Nadezhda N. Erzakova [1], Andrei V. Chikiryaka [5], Mikhail P. Shcheglov [5], Houssain Baalbaki [1] and Alexey S. Olshukov [1]

1 Research and Development Center for Advanced Technologies in Microelectronics, National Research Tomsk State University, 634050 Tomsk, Russia
2 Fokon LLC, 248035 Kaluga, Russia
3 Laboratory of Optical Crystals LLC, 634040 Tomsk, Russia
4 Vladimir Zuev Institute of Atmospheric Optics, Russian Academy of Sciences, Siberian Branch, 634055 Tomsk, Russia
5 Ioffe Institute of the Russian Academy of Sciences, 194021 Saint Petersburg, Russia
* Correspondence: almaev_alex@mail.ru

Abstract: TiO_2 films of 130 nm and 463 nm in thickness were deposited by ion beam sputter deposition (IBSD), followed by annealing at temperatures of 800 °C and 1000 °C. The effect of H_2, CO, CO_2, NO_2, NO, CH_4 and O_2 on the electrically conductive properties of annealed TiO_2 thin films in the operating temperature range of 200–750 °C were studied. The prospects of IBSD deposited TiO_2 thin films in the development of high operating temperature and high stability O_2 sensors were investigated. TiO_2 films with a thickness of 130 nm and annealed at 800 °C demonstrated the highest response to O_2, of 7.5 arb.un. when exposed to 40 vol. %. An increase in the annealing temperature of up to 1000 °C at the same film thickness made it possible to reduce the response and recovery by 2 times, due to changes in the microstructure of the film surface. The films demonstrated high sensitivity to H_2 and nitrogen oxides at an operating temperature of 600 °C. The possibility of controlling the responses to different gases by varying the conditions of their annealing and thicknesses was shown. A feasible mechanism for the sensory effect in the IBSD TiO_2 thin films was proposed and discussed.

Keywords: ion beam sputter deposition (IBSD); TiO_2; gas sensor

Citation: Almaev, A.V.; Yakovlev, N.N.; Kushnarev, B.O.; Kopyev, V.V.; Novikov, V.A.; Zinoviev, M.M.; Yudin, N.N.; Podzivalov, S.N.; Erzakova, N.N.; Chikiryaka, A.V.; et al. Gas Sensitivity of IBSD Deposited TiO_2 Thin Films. *Coatings* **2022**, *12*, 1565. https://doi.org/10.3390/coatings12101565

Academic Editor: María Dolores Fernández Ramos

Received: 16 September 2022
Accepted: 11 October 2022
Published: 17 October 2022

1. Introduction

Titanium oxide (TiO_2) belongs to the class of wide-gap semiconductors with intrinsic *n*-type conductivity [1–7]. Gas sensors [1–3,8–10], photodetectors and solar panels [11,12], memristors [13] and photocatalysts [14,15] have been developed. based on TiO_2 films, due to their having structural, optical, electrically conductive and catalytic properties, high thermal and chemical stability, being relatively cheap, with good availability. The metastable anatase and brookite phases of TiO_2 at the temperatures of 600–1000 °C transform into the stable rutile phase [9]. All three phases of TiO_2 exhibit sensitivity to gases, depending on the method of their preparation, and their electrical, structural and dimensional parameters [1–3,8–10]. Resistive [1–3,8–10] and capacitive [16,17] sensors based on TiO_2 are being developed, including for high operating temperature applications. The resistive sensors are easy to implement and relatively cheap. In many cases, they consist of a semiconductor film on the surface of an insulating substrate with metal contacts. The resistive sensor also includes a heater to stimulate physical and chemical processes between the film surface and gas molecules.

TiO_2 thin films are highly sensitive to gases due to an increase in the contribution of surface conductance, which largely depends on the charge state of the film surface [2,3,10,18]. One of the techniques to produce thin films of metal oxide semiconductors is physical vapor deposition (PVD), including thermal evaporation (EV), pulsed laser deposition (PLD), magnetron sputtering (MS), and ion beam sputter deposition (IBSD). These methods are

used to deposit high-quality thin films of metal oxide semiconductors for various applications, with a wide range of thicknesses, to combine the production of thin films with microelectronic technologies, and to modify the composition of, and control the properties of, films by varying the conditions of their deposition [19–28]. IBSD is distinguished by the highest energies of forming particles. as well as a large number of parameters affecting the deposition process and the possibility of achieving a higher vacuum in the operating mode [27–34]. This allows fine varying of the electrically conductive, structural, optical, mechanical, and other properties of the films during deposition, and to deposit more uniform layers in thickness and composition over large areas of the substrates. The IBSD thin films are characterized by better adhesion, denser structure, fewer defects, close to ideal stoichiometry and higher purity, compared to films deposited by other PVD methods.

The gas-sensitive properties of metal oxide semiconductor thin films fabricated by the IBSD method (see Table 1) have been much less studied than those obtained by the MS and PLD. In Table 1, d is the film thickness; n_g is the target gas concentration; T_{MAX} is the operating temperature of maximum response; and S is the response to gas. The ratio R_{air}/R_g was chosen as the film's response to the gas, where R_{air} is the film's resistance in pure air and R_g is the film resistance in a mixture of air + target gas. The thicknesses of the In_2O_3, SnO_2, and MoO_3 films did not exceed 500 nm and for most films d were below 100 nm. The films described above were characterized by the absence of pores and grain structure. but demonstrated a high response to low concentrations of reducing gases [35–38]. In ref [38] it was shown that the response to 0.01 vol. % NH_3 of MoO_3 films, deposited by IBSD with a less developed surface, was 2.5 times higher than the response of films obtained by the sol–gel method. The IBSD was also used to deposit layers of catalyst metals on film surfaces with a thickness of a few nanometers. This made it possible to significantly increase S and reduce T_{MAX} [33,37]. The optimal value of d for the SnO_2 film thickness was 100 nm [35]. The sensitivity mechanism of the IBSD synthesized films without a grain structure is rather similar to the sensitivity mechanism of single-crystalline metal oxide semiconductor thin film [39].

Table 1. Gas sensitive characteristics of IBSD metal oxide semiconductors (MOS) thin films.

MOS	d (nm)	Gas	n_g (vol. %)	T_{MAX} (°C)	S	Ref.
In_2O_3	40	Isoprene	25×10^{-4}	432	1.02	[33]
Au/In_2O_3				364	2.82	
Pt/In_2O_3				255	2.51	
Pd/In_2O_3				196	6.31	
SnO_2	10	H_2	0.1	350	20	[35]
	20				25	
	50				60	
	100				70	
	200				30	
	500				20	
SnO_2	50	C_4H_{10}	0.5	400	4	[36]
Pt/SnO_2					4.5	
SnO_2:Ca					2.5	
Pt/SnO_2:Ca					2.3	
SnO_2	50	CH_4	0.5	400	1.75	[37]
SnO_2:Ca					1.4	
MoO_3	-	NH_3	0.01	450	4	[38]

Meanwhile, there are no publications devoted to the gas sensitive properties of IBSD TiO_2 thin films. Refs [29–32] investigated of the impact of IBSD parameters on the optical, structural, and mechanical properties of TiO_2 thin films. Argon, oxygen, and xenon ions were used to sputter the Ti and TiO_2 targets. It was shown that the properties of the films were weakly affected by the type of targets, energy, and type and incidence angle of ions. However, the scattering geometry had a significant effect on the film's properties.

Our present research is devoted to a comprehensive study on the structural, electrical, and, most of all, gas-sensitive properties of pure TiO_2 thin films, obtained by the IBSD technique.

2. Experimental Methods

TiO_2 thin films were fabricated by the IBSD technique using Aspira-200 equipment with an annular beam of ion source. The sputtered target was a 5-inches Ti disk, with a purity of 99.995 wt. %. The diameter of the ion beam focused on the target was ~25 mm. Ar (99.995 vol. %) and O_2 (99.7 vol. %) were used as the working gases. The ratio of partial flows Ar/O_2 was $\frac{1}{2}$ at a total flow of 30 cm^3/min. Polished polycrystalline sapphire plates were chosen as substrates. Prior to deposition of TiO_2 films, the substrates were cleaned using high purity acetone. and subsequently washed in bi-distilled water. The substrates were cleaned by means of an auxiliary ion source with a source power of ~40 W and an ion energy of ~150 eV for 10 min before film deposition. The substrate temperature during film growth was kept at 100 °C. The films were deposited at a gas pressure in the chamber of 5×10^{-4} Pa. The thicknesses of the TiO_2 films were 130 nm and 463 nm. The average deposition rate of the TiO_2 films was 0.3 Å/s. After sputtering, the TiO_2 thin films were annealed at T_{ann} = 800 °C and 1000 °C in air for 60 min. As-deposited TiO_2 films are amorphous [28]. TiO_2 films are of interest for high-temperature operating gas sensors with T > 600 °C [40]. Annealing temperatures of T_{ann} = 800 °C and 1000 °C are known to prevent changes in the microstructure of the films during high temperature heating. Pt contacts were deposited on the TiO_2 film surfaces through a mask to measure the gas sensitive properties.

The surface morphology of the films was studied by atomic force microscopy (AFM). X-ray diffraction analysis (XRD) was performed to determine the phase composition of the films. The XRD measurements were carried out using a diffractometer with CuKα radiation operated at 40 kV and 30 mA. The X-ray source wavelength was 1.54 Å. Transmission spectra, in the wavelength range of λ = 310–485 nm, were studied for TiO_2 films deposited on single-crystalline sapphire substrates.

The current–voltage (I–V) characteristics and time dependences of the sample resistance under exposure to various gases were measured by a Keithley 2636A source-meter and a hermetic Nextron MPS-CHH micro-probe station. The measurements were carried out under dark conditions and in a flow of dry pure air, or in a gas mixture of dry pure air + target gas. H_2, CO, CO_2, NO_2, NO, CH_4 and O_2 were selected as target gases. A mixture of N_2 and O_2 was used to study the film sensitivity to oxygen. The flow rate of gas mixtures through the measurement chamber was maintained at 1000 cm^3/min. The source of dry pure air was a special generator. The concentration of the target gas in the mixture was controlled by a gas mixture generator with a Bronkhorst gas mass flow controller. The relative error of the gas flow rate did not exceed 1.5%. The samples were mounted on a hot stage and heated to the desired operating temperature, T_{oper}, in the range from RT to 750 °C, where RT was the room temperature. The T_{oper} was controlled by the Nextron MPS-CHTC controller. The accuracy of the T_{oper} setting was ±0.1 °C. The applied voltage U to the samples was 5 V.

3. Results and Discussion

3.1. Structural Properties of TiO_2 Films

The surface morphology of the as-deposited films consisted of grains, which, after annealing, formed large agglomerates (illustrated in Figure 1). The presence of a grain structure for films without annealing was caused by the low quality of the polycor substrate,

which was considered appropriate to use for the manufacture of cheap sensor chips. The surface morphology parameters of the TiO_2 thin films are compared in Table 2, where D_a was the size of TiO_2 agglomerates along the substrate plane and D_g was the TiO_2 grain size along the substrate plane. An increase in d and T_{ann} led to an increase in D_a and D_g.

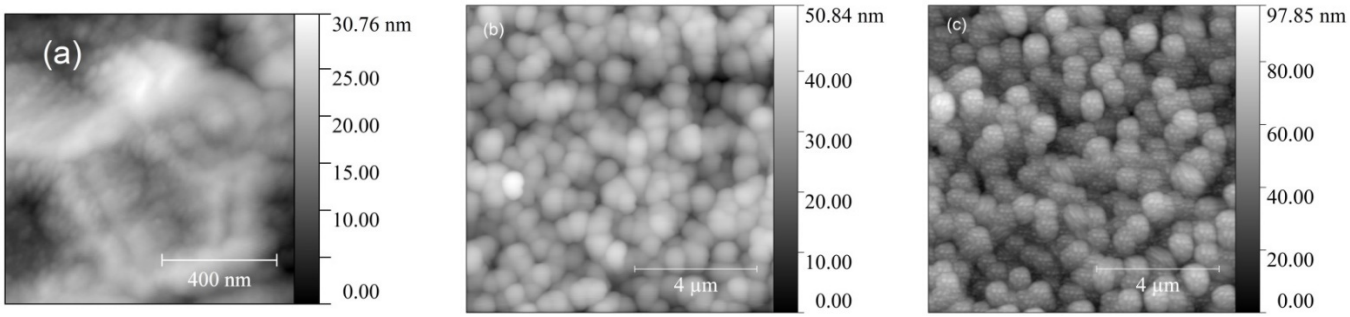

Figure 1. AFM images of TiO_2 thin films surface at d = 463 nm and T_{ann} = 0 (**a**), T_{ann} = 800 °C (**b**); T_{ann} = 1000 °C (**c**).

Table 2. Surface microrelief parameters of TiO_2 thin films.

d (nm)	T_{ann} (°C)	D_a (nm)	D_g (nm)
130	0	-	10–30
	800	320–550	100
	1000	500–700	125
463	0	-	10–30
	800	350–600	100–110
	1000	600–800	150

The XRD spectra of the as-prepared films, exhibited in Figure 2, demonstrated many low-intensity peaks that could be associated with different crystallographic planes of the corundum Al_2O_3 phase. The as-deposited films were amorphous and the XRD spectra of these films corresponded to polycrystalline sapphire substrate. After annealing, the positions of the Al_2O_3 peaks persisted, but the intensity of these peaks decreased. Peaks at $2\theta = 39.7^\circ$ and $2\theta = 46.17^\circ$ on the XRD spectra appeared after annealing. The second peak was associated with the (202) crystallographic plane of the Al_2O_3 [41]. The high-intensity peak at $2\theta = 39.7^\circ$ could be associated with the (200) crystallographic plane of the rutile TiO_2 phase. The position of this peak did not depend on T_{ann}. There was a slight shift in the positions of the peaks to the right, probably due to the presence of elastic deformations in the films after high-temperature annealing [42]. The XRD spectra of IBSD TiO_2 thin films differed sharply from the spectra of TiO_2 films and nanosized structures obtained by other methods [14,43–46]. The intense peak at $2\theta = 38.65^\circ$, associated with the (200) crystallographic plane of the TiO_2 rutile phase, was observed for MS deposited TiO_2 thin films annealed at T_{ann} = 900 °C [47]. The authors were unable to find data on the study of the XRD spectra of the IBSD deposited TiO_2 thin films.

Direct optical transitions take place for TiO_2 films, regardless of T_{ann}, that is characteristic for the rutile phase [48,49]. An increase in T_{ann} from 800 °C to 1000 °C led to a decrease in the energy of band gap E_g from 3.5 eV to 3.2 eV. The value $E_g = 3.2\ eV$ is typical for the rutile TiO_2 phase [48,49]. The higher value of E_g at T_{ann} = 800 °C could be explained by the existence of a small fraction of the anatase crystalline phase with a larger E_g in the TiO_2 film's structure.

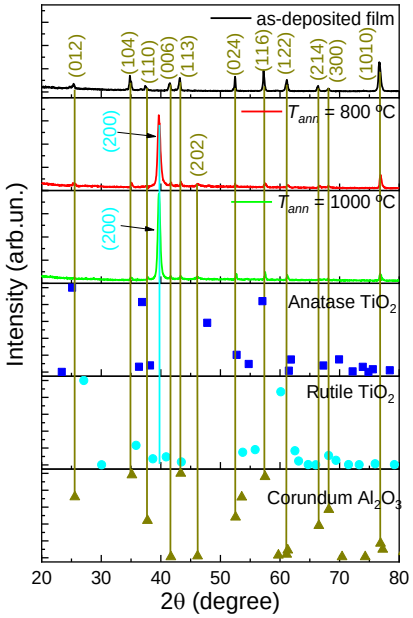

Figure 2. XRD spectra of TiO_2 films annealed at T_{ann} = 800 °C and 1000 °C.

Thus, it could be concluded that the annealed films composed of the rutile phase of TiO_2. TiO_2 films annealed at T_{ann} = 800 °C might contain a small amount of the anatase modification. Increasing T_{ann} up to 1000 °C led to the final transition of the TiO_2 films into the high-temperature rutile phase.

3.2. Electrically Conductive Properties of TiO_2 Thin Films in Dry Pure Air

The *I–V* characteristics of TiO_2 thin films with Pt contacts were linear in the ranges of U = 0–20 V, T_{oper} = 200–750 °C and T_{oper} = 400–750 °C after annealing at T_{ann} = 800 °C and 1000 °C, respectively. For TiO_2 films annealed at T_{ann} = 800 °C the differential conductance G_d increased exponentially with T_{oper} from 200 °C to 750 °C without any features characteristic of MOS thin films [50]. A decrease in the film thickness from 463 nm to 130 nm led to an increase in G_d by 1–2 orders of magnitude. An increase in T_{ann} up to 1000 °C led to a decrease in G_d by 40 times at d = 130 nm and by 700 times at d = 463 nm. The activation energies of conduction ΔE_d did not depend on d (Figure 3), at T_{ann} = 800 °C ΔE_d = 1.29 ± 0.08 eV and at T_{ann} = 1000 °C ΔE_d = 2.36 ± 0.05 eV.

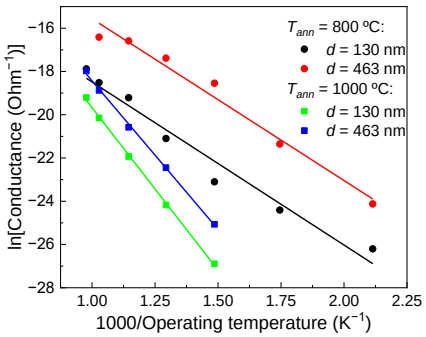

Figure 3. Arrhenius curves for TiO_2 films after annealing at T_{ann} = 800 °C and 1000 °C.

The ΔE_d of films annealed at T_{ann} = 800 °C was close to the values for bulk samples obtained by ceramic technology with annealing at 800 °C [51]. The activation energy of films annealed at T_{ann} = 1000 °C coincided with the value of ΔE_d for single-crystal bulk samples obtained by the Verneuil melt method [52]. Such values of ΔE_d are typical for

high-temperature treatments, or grown methods, and are caused by the presence of oxygen vacancies in TiO_2.

3.3. The Effect of Oxygen on the Electrically Conductive Properties of TiO_2 Thin Films

TiO_2 films are of interest for the development of high operating temperature O_2 sensors for extreme environments [53–55], due to their high chemical and thermal stability. The effect of O_2 led to a reversible increase in the resistance of TiO_2 thin films placed in an atmosphere of dry N_2 (Figure 4). The rise of the resistance of the film under exposure to O_2, and the drop of resistance after this exposure, were approximated by the following functions, respectively:

$$R(t) = R_{Ost} - A\exp[-t/\tau_1], \quad (1)$$

$$R(t) = R_{Nst} + B\exp[-t/\tau_2], \quad (2)$$

where R is the resistance of a TiO_2 thin film, t is time and R_{Ost} and R_{Nst} are the stationary values of the film resistance in the N_2 + O_2 mixture and in N_2, respectively. A and B are constants; τ_1 and τ_2 are time constants. The operation speed of gas sensors is determined by response t_{res} and recovery t_{rec} times. These values are given by the relaxation times of adsorption τ_A and desorption τ_D of gas molecules on the solid surface, τ_A & $\tau_D \sim \exp[(E_D–E_A)/(2kT)]$, where E_D and E_A are the activation energies of desorption and adsorption processes of gas molecules on the semiconductor surface, k is the Boltzmann constant, and T is the absolute temperature of the semiconductor. The values, τ_A, τ_D, and, hence, t_{res}, t_{rec} sharply decrease with T_{oper}. The values τ_1 and τ_2 are related to τ_A and τ_D, respectively. From Equations (1) and (2), the exponents at $t \geq 2.3\tau_1$ and $t \geq 2.3\tau_2$ can be neglected. The resistance of the TiO_2 thin film achieved R_{Ost} and R_{Nst} at $t \geq 2.3\tau_1$ and $t \geq 2.3\tau_2$. Thus, $t_{res} = 2.3\tau_1$ and $t_{rec} = 2.3\tau_2$. Estimates of t_{res} and t_{rec} for TiO_2 thin films at T_{oper} = 750 °C are presented in Table 3.

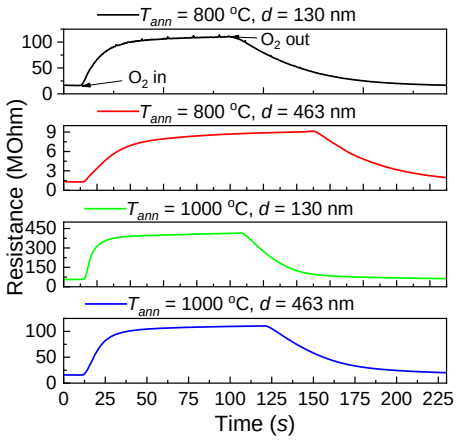

Figure 4. Time dependences of the TiO_2 thin films resistances upon exposure to 40 vol. % O_2 and T_{oper} = 750 °C.

Table 3. Response and recovery times of TiO_2 thin films upon exposure to 40 vol. % O_2 and T_{oper} = 750 °C.

T_{ann} (°C)	d (nm)	t_{res} (s)	t_{rec} (s)
800	130	35.0	85.3
	463	54.7	85.1
1000	130	12.6	47.8
	463	23.9	92.6

Increasing T_{ann} at a fixed value of d and decreasing d at a fixed value of T_{ann} led to a decrease in t_{res}. Changing the film thickness at T_{ann} = 800 °C did not affect t_{rec}, but, at T_{ann} = 1000 °C, a decrease in the film's thickness led to a decrease in t_{rec} by about 2 times.

At d = 130 nm, an increase in T_{ann} led to a significant decrease in t_{rec} by 1.8 times, and at d = 463 nm, there was a slight increase in t_{rec}. The increase in t_{res} and t_{rec} with increasing d and fixed T_{ann} are explained by the formation of a more developed surface. It slows down the diffusion of oxygen molecules and atoms, on the one hand, and of oxygen vacancies, on the other hand [56]. The decrease in t_{res} with an increase in T_{ann} and a fixed thickness was caused by an increase in the size of grains and agglomerates, which led to the opposite effect. It is worth noting that t_{res} and t_{rec} contained the time required to establish the stationary state of the atmosphere in the measuring chamber, which, according to our estimates, could reach 6 s.

The following ratio, S_O, was chosen as the film response to O_2:

$$S_O = R_{Ost}/R_{Nst}. \quad (3)$$

Films annealed at T_{ann} = 800 °C showed sensitivity to O_2 in the range of T_{oper} = 300–750 °C (shown in Figure 5). For these films the maximum response was observed at T_{oper} = 750 °C. At T_{oper} = 700–750 °C films with d = 130 nm were characterized by the highest responses to O_2. In the range of T_{oper} = 300–600 °C TiO_2 thin films with a thickness of 463 nm and annealed at T_{ann} = 800 °C demonstrated a slightly higher response to O_2.

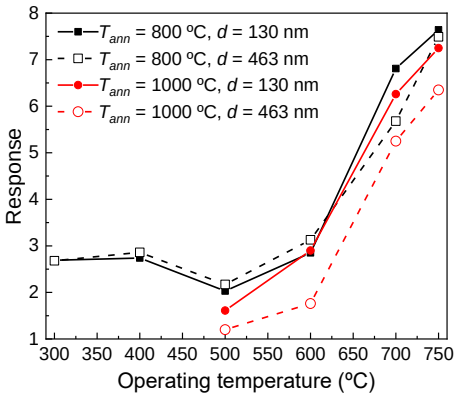

Figure 5. Dependences of the response to 40 vol. % O_2 on operating temperature.

For TiO_2 thin films annealed at T_{ann} = 1000 °C the response to O_2 was measured in the range of T_{oper} = 500–750 °C. At T_{oper} = 300–500 °C and these films were not sensitive to O_2. An increase in T_{ann} led to a decrease in the response to O_2 at fixed values of d, due to the effect of changes in the surface microrelief. The films were not sensitive to O_2 at T_{oper} = 300–500 °C for the same reason. A decrease in the response at fixed T_{oper} with d was observed, due to an increase in the contribution of bulk conductivity. The maximum responses to O_2 for these films within T_{oper} range of 500–750 °C took place at T_{oper} = 750 °C. We believe that the response for these films would increase with a further increase in T_{oper} [1–3,8–10]. Measurements at T_{oper} >750 °C were limited by the capabilities of measuring equipment.

The dependences of the TiO_2 thin film responses to the O_2 concentration at T_{oper} = 750 °C (displayed in Figure 6) were approximated by the power function $S_O \sim {n_{O2}}^l$, where n_{O2} is the O_2 concentration and l is the power index. A change in the film thickness at a fixed value of T_{ann} had little effect on the value of l (Table 4). An increase in T_{ann} led to a decrease in l by ~0.025.

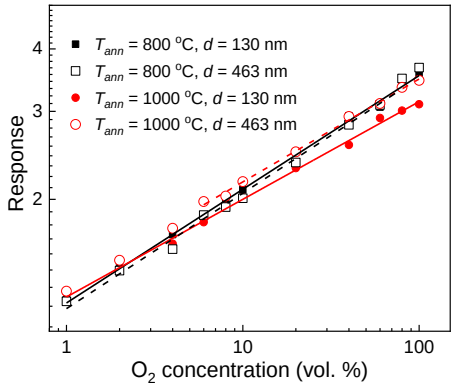

Figure 6. Dependences of the response on the O_2 concentration at T_{oper} = 750 °C.

Table 4. Power indexes l for TiO_2 thin films at T_{oper} = 750 °C.

T_{ann} (°C)	d (nm)	l
800	130	0.227 ± 0.004
	463	0.235 ± 0.006
1000	130	0.195 ± 0.003
	463	0.212 ± 0.002

3.4. Sensitivity of TiO_2 Thin Films to Reducing and Oxidizing Gases

At T_{oper} = 600 °C and 750 °C the responses of TiO_2 films to fixed concentrations of reducing and oxidizing gases were measured (Figure 7). The resistance of the films decreased when exposed to reducing gases: CO, CH_4, and H_2. Under exposure to oxidizing gases, CO_2, NO and NO_2, the resistance of the films reversibly increased. The responses to reducing gases were determined by the following formula:

$$S = R_{airst}/R_{gst}, \quad (4)$$

where R_{airst} and R_{gst} are stationary values of the TiO_2 film resistance in dry pure air and in a mixture of dry pure air + target gas, respectively. The responses to oxidizing gases were determined by the inverse relation of (4).

TiO_2 films at d = 463 nm and T_{ann} = 800 °C demonstrated relatively high responses to 1 vol. % H_2 and 0.01 vol. % NO_2. TiO_2 films at d = 130 nm and T_{ann} = 1000 °C demonstrated relatively high responses to 1 vol. % CO, CO_2 and CH_4. At T_{oper} = 600 °C responses to 40 vol. % O_2 were lower than the responses to 1 vol. % H_2, regardless of the film thickness and T_{ann}, as well as being lower than the responses of TiO_2 films at d = 130 nm and T_{ann} = 1000 °C to 1 vol. % CO, CO_2 and CH_4. Responses of TiO_2 films to fixed concentrations of other gases, in comparison with the response to 40 vol. % O_2 at different d and T_{ann}, were comparable or lower. Increasing the operating temperature of TiO_2 thin films up to 750 °C, regardless of d and T_{ann}, led to a decrease in responses to all gases, except for O_2 and CH_4. Responses to O_2 and CH_4 increased with T.

A more significant Increase in the response to O_2, as well as a decrease in responses to other gases, should be expected with a further increase in T_{oper}. It is believed that at T_{oper} > 750 °C the sensitivity to gases is realized due to the interaction with oxygen vacancies [53–55]. In this operating temperature range the sensors should be selectively sensitive to O_2. However, chemisorption of gas molecules on the semiconductor surface and their interaction with semiconductor defects can occur at T_{oper} >750 °C. It often leads to the manifestation of high operating temperature sensitivity to reducing gases. Due to safety requirements and technical limitations the comparison of responses to the same concentration of different gases was not experimentally studied. For this reason, the

sensitivity of TiO_2 thin films to oxygen β_O and other gases β was compared, using the following ratios, respectively:

$$\begin{gathered} \beta_O = (R_{Ost} - R_{Nst})/n_{O2}, \\ \beta = (R_{airst} - R_{gst})/n_g \text{ for reducing gases,} \\ \beta = (R_{gst} - R_{airst})/n_g \text{ for oxidizing gases.} \end{gathered} \quad (5)$$

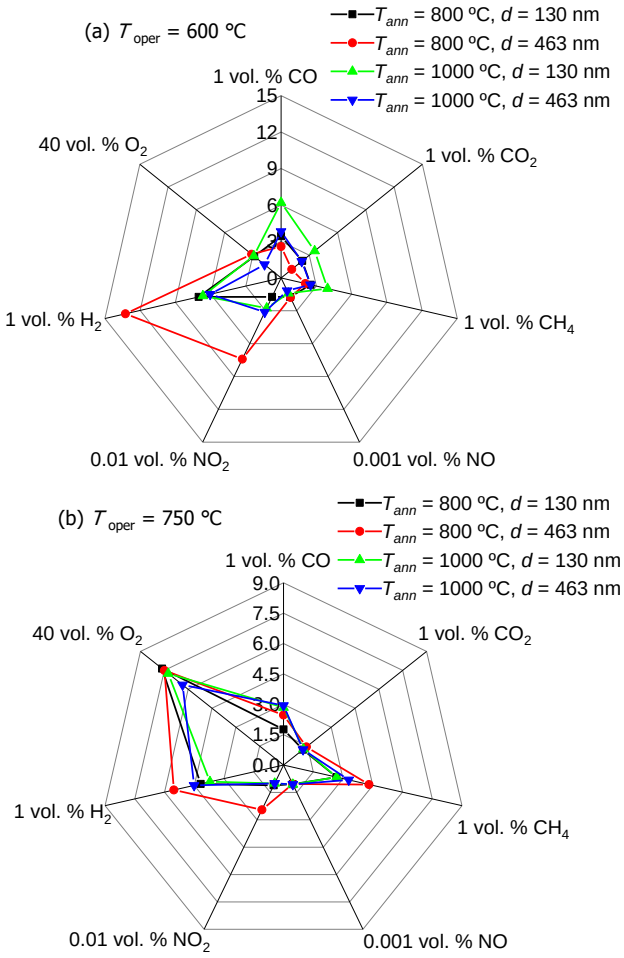

Figure 7. Responses to fixed concentrations of various gases at T_{oper} = 600 °C (**a**) and T_{oper} = 750 °C (**b**).

It is worth noting that the estimates of values β_O and β (Figure 8) did not take into account the possible saturation of the gas-sensitive characteristics of the films under exposure to used gas concentrations. The films were characterized by the highest sensitivity to nitrogen oxides and showed approximately the same sensitivity to CO, CO_2, CH_4 and H_2 at T_{oper} = 600 °C, regardless of d and T_{ann}. The lowest sensitivity of TiO_2 films was realized when exposed to O_2. An increase in T_{oper} up to 750 °C led to a decrease in β_O and β, due to a decrease in the base resistance. In this case, the ratios between the sensitivities to different gases were preserved. TiO_2 films at d = 130 nm and T_{ann} = 1000 °C were characterized by the highest sensitivity to gases. TiO_2 films at d = 463 nm and T_{ann} = 800 °C demonstrated the lowest sensitivity to gases.

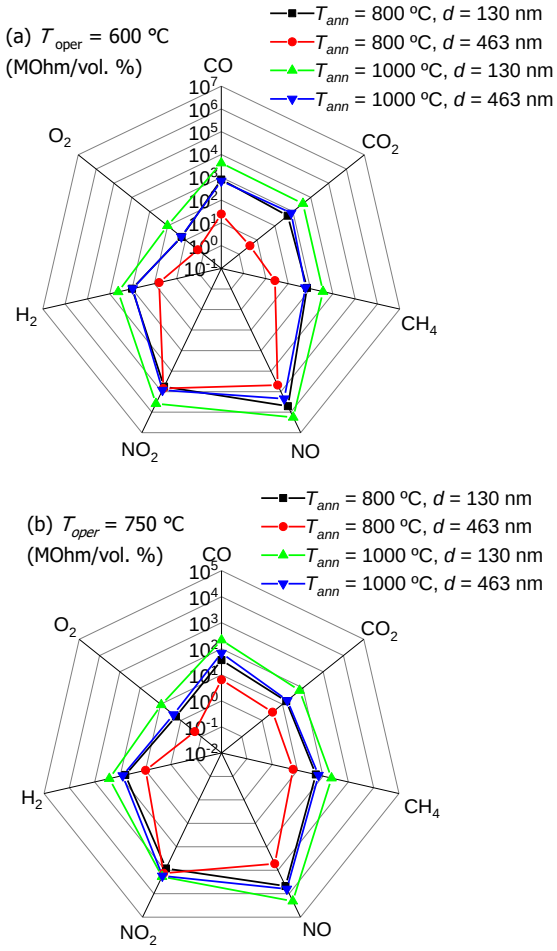

Figure 8. Sensitivity of TiO_2 thin films to various gases at T_{oper} = 600 °C (**a**) and T_{oper} = 750 °C (**b**).

The repeatability of IBSD TiO_2 thin film characteristics was investigated under cyclic exposure to H_2 and O_2 gases (see Figure 9). Obviously, an increase in the thickness of films at a fixed T_{ann} value led to an improvement in the repeatability of resistance and response of samples when exposed to H_2. The standard deviations of S at d = 463 nm were 5% and 2% at T_{ann} = 800 °C and 1000 °C, respectively. Response to H_2 for films at d = 130 nm and T_{ann} = 800 °C increased with each cycle of gas exposure, due to an increase in R_{airst}. For these films S increased 1.4 times after 6 cycles of H_2 exposure. Films at d = 130 nm and T_{ann} = 1000 °C were not characterized by high repeatability of the resistance and S under exposure to H_2. The IBSD TiO_2 thin films demonstrated high reproducibility of resistance and S_O under cyclic exposure to O_2. The standard deviations of S_O when exposed to O_2 were 1–2%. The reason for the instability of the IBSD fabricated TiO_2 thin film characteristics at d = 130 nm might be the process of Ti reduction by hydrogen. This process was considered in detail for MS deposited SnO_2 thin films at d = 100 nm [57]. The density of adsorption centers on the TiO_2 film surface increases at Ti reduction by hydrogen. Oxygen is primarily chemisorbed onto these newly formed adsorption centers, which leads to an increase in R_{airst} and S. It is worth mentioning that this process became significant with a decrease in the film thickness, as the contribution of surface electrically conductance increased. The contribution of this process became insignificant with increasing d.

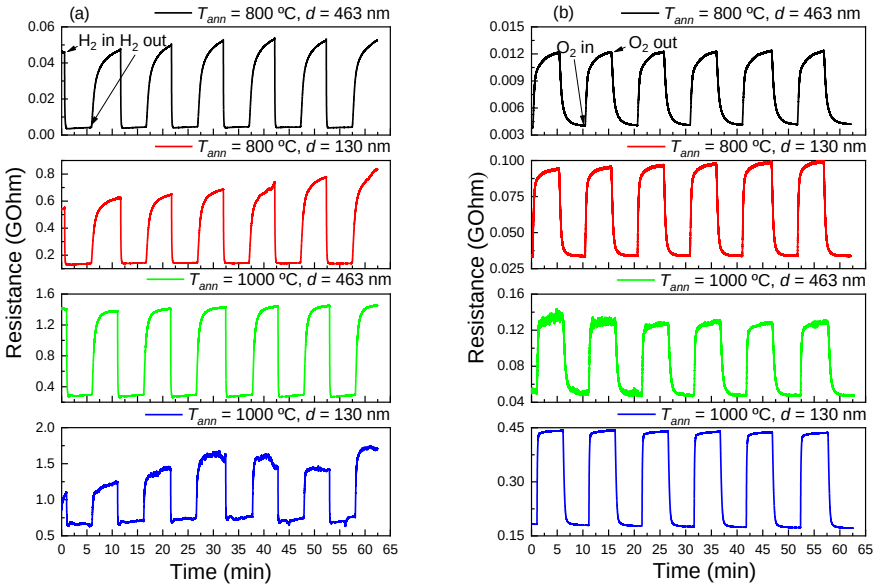

Figure 9. Time dependences of the TiO_2 thin films resistances upon exposure to 1 vol. % H_2 at T_{oper} = 600 °C (**a**) and upon exposure to 40 vol. % O_2 at T_{oper} = 750 °C (**b**).

Thus, the IBSD TiO_2 thin films demonstrated high sensitivity to H_2, NO_2 and exhibited potential for the development of O_2 sensors operating at high temperatures. For this reason, a comparison of sensitivity to O_2, H_2 and NO_2 for thin films obtained by different CVD and PVD methods is presented in Table 5, where CVD represents chemical vapor deposition. In Table 5, RFMS is radio-frequency magnetron sputtering, DCMS is direct-current magnetron sputtering, MOCVD is metalorganic chemical vapor deposition, EBE + oxidation is electron beam evaporation with following oxidation and ALD is atomic laser deposition.

Table 5. Comparison of sensitivity to O_2, H_2 and NO_2 for thin films deposited by different CVD and PVD methods.

Methods	d (nm)	n_g (vol. %)	T_{oper} (°C)	S	Ref.
		O_2			
RFMS	50	0.6	500	1.14	[58]
DCMS	60	10	RT	76	[59]
IBSD	130	40	750	7.64	This work
		H_2			
DCMS	50	1	450	~10^4	[47]
DCMS	160	1	120	10^7	[60]
RFMS	~300	1	175	1.8	[61]
MOCVD	71	1	100	1.3	[62]
EBE + oxidation	25	0.05	500	91	[63]
DCMS	400	3	150	1.1×10^4	[64]
IBSD	463	1	600	13.25	This work
		NO_2			
RFMS	10	0.05	RT	1.021	[65]
ALD	8	0.1	RT	7.5×10^{-7} *	[66]
IBSD	463	0.01	600	7.41	This work

* The response was determined from the frequency properties.

The IBSD deposited TiO_2 thin films were characterized by high response to O_2 at high operating temperatures. In refs. [58,59] the sensitivity to O_2 of much thinner TiO_2 films were studied. UV irradiation of films was employed to increase the response at RT [59]. At the same time, t_{res} was 360 s, which gave rise to significantly larger t_{res} and t_{rec} for the IBSD TiO_2 thin films (see Table 3).

The response to H_2 of IBSD deposited TiO_2 thin films was not high in comparison with other samples. The advantage of IBSD deposited TiO_2 thin films was relatively high sensitivity at high operating temperatures, which is of interest for high operating temperature sensor applications. The high responses for DCMS and RFMS deposited films are due to the formation of Pt, Pd and PdO catalytic layers, as well as a fine-grained structure with D_g = 15 nm [60,61,64]. In most papers, t_{res} and t_{rec} reached several *min* and even tens of min [47,62,64]. The repeatability of the TiO_2 thin film characteristics when exposed to H_2 was not practically considered. For IBSD deposited TiO_2 thin films annealed at T_{ann} = 1000 °C with d = 130 nm the lowest t_{res} and t_{rec} were 23.4 s and 108.6 s, respectively.

IBSD deposited TiO_2 thin films demonstrated the highest response to NO_2. In references [65,66], TiO_2 thin films showed sensitivity to gas at RT. However, the S was low, t_{res} and t_{rec} were hundreds of s. In ref [66] the authors analyzed the effect of NO_2 on frequency properties of TiO_2 thin films. The frequency response was low.

It can be concluded that IBSD deposited TiO_2 thin films are of interest for high operating temperature sensor applications. At the same time, in most of the research TiO_2 thin films were modified with additives or irradiated with UV. The characteristics of such films and IBSD deposited TiO_2 thin films are comparable in most cases. The capabilities of IBSD for the modification of TiO_2 thin films [33,37] may allow the achieving of superior performance for sensors in the future.

3.5. Sensory Effect

Estimates for TiO_2 thin films with a rutile structure showed that in the range of T_{oper} = 300–750 °C, the ratio $L_D > D_g/2$ took place, where L_D is the Debye length. The possible inclusion of the anatase phase in TiO_2 films annealed at T_{ann} = 800 °C did not significantly affect the ratio between L_D and $D_g/2$. Thus, the transport of charge carriers in TiO_2 films was not affected by the presence of a potential barrier at the boundaries of small grains and large agglomerates that formed after annealing of the films. This is typical for IBSD deposited MOS films, as seen in Ref. [39].

The power index for films at T_{oper} = 750 °C l = 0.20–0.23 (Table 4). The values of l at other identical conditions were determined by the film surface microrelief [67,68], which changed with varying annealing conditions. It was shown in ref [53] that $l = \frac{1}{4}$, 1/5 and 1/6 occurred at T_{oper} > 800 °C and were characteristic for the interaction of oxygen molecules with TiO_2 bulk defects, namely, oxygen vacancies and interstitial Ti atoms. A significant contribution to the gas sensitivity of TiO_2 films, concerning the interaction of gas molecules, oxygen vacancies and other bulk defects at $T_{oper} \leq$ 750 °C, could be neglected due to diffusion limitations [53–55]. The conductivity of the film changes as a result of chemisorption of gas molecules on the semiconductor surface. Oxygen molecules are chemisorbed on the film surface in an air atmosphere. Oxygen captures electrons from the conduction band of the semiconductor and forms a layer depleted in charge carriers on the film pre-surface region. Oxygen is chemisorbed on the semiconductor surface in the molecular $O_2^-{}_{(c)}$ and atomic $O^-{}_{(c)}$, $O_2^-{}_{(c)}$ forms [69]. The molecular form of chemisorbed oxygen dominated at T_{oper} < 150 °C. With a further increase in T, dissociative adsorption of oxygen molecules took place and the predominant forms of chemisorbed oxygen were $O^-{}_{(c)}$ and $O_2^-{}_{(c)}$. The obtained values of l ~0.25 indicated the predominance of $O_2^-{}_{(c)}$ on the surface of TiO_2 thin films. It is worth noting that the $O^-{}_{(c)}$ form was the most reactive. A negative charge on the surface of the n-type film led to the upward bending of energy bands eV_s, where vs. is the surface potential, and e is the electron charge. In the value $eV_s \sim N_i^2$, N_i is the surface density of chemisorbed oxygen ions. The mechanism of the sensory effect described in ref [39] could be used for the IBSD TiO_2 thin films. The total

conductance of the TiO_2 film was $G_t = G_b + G_s$, where G_b is the bulk conductance; G_s is the surface conductance. The value of G_s depends on the chemisorption of gas molecules on the semiconductor surface.

The expression describing the relationship between G_t and vs. for an *n*-type semiconductor at vs. > 0 has the following form ref [39]:

$$G_t = G_b \times [1 - (L_D/d) \times [eV_s/(kT)]] \quad (6)$$

It can be noted from expression (6) that an increase in the oxygen concentration in the chamber with TiO_2 films led to a decrease in total conductance. Expression (6) took place at $L_D/d << 1$ and a small band bending $eV_s/(kT) << 1$. According to our estimates these inequalities were valid for our experimental conditions.

Interactions of previously chemisorbed $O^-_{(c)}$ and molecules of reducing gases can be represented in the following forms:

$$\begin{gathered} H_2 + O^-_{(c)} \rightarrow H_2O + e; \\ CO + O^-_{(c)} \rightarrow CO_2 + e, \\ CH_4 + 4O^-_{(c)} \rightarrow CO_2 + 2H_2O + 4e. \end{gathered} \quad (7)$$

As a result of these reactions N_i, and eV_s decrease, and electrons return to the conduction band of semiconductors. The reaction products between reducing gases and $O^-_{(c)}$ are desorbed as neutral CO_2 and H_2O molecules. The following reactions can occur on the semiconductor surface when exposed to oxidizing gases CO_2, NO_2, and NO, [70,71]:

$$\begin{gathered} NO_2 + S_a + e^- \rightarrow NO_2^-, \\ NO_2 + O^-_{(c)} \rightarrow NO_3^-, \\ NO + S_a + e^- \rightarrow NO^-, \\ NO + O^-_{(c)} \rightarrow NO_2^-, \\ CO_2 + S_a + e^- \rightarrow CO_2^-. \end{gathered} \quad (8)$$

Molecules of oxidizing gases can be chemisorbed onto the free adsorption center S_a without the interaction with O^-_c ions capturing electrons from the conduction band of the semiconductor. In mixtures of air + NO_2 $eV_s \sim (N_{iA} + N_{NO2})^2$, air + NO $eV_s \sim (N_{iA} + N_{NO})^2$ and air + CO_2 $eV_s \sim (N_{iA} + N_{CO2})^2$, where N_{iA} is the surface density of chemisorbed oxygen ions in the air atmosphere; N_{NO2}, N_{NO} and N_{CO2} are the surface densities of chemisorbed NO_2^-, NO^- & CO_2^--ions, respectively. An additional negative charge on the surface of TiO_2 films leads to a greater increase in eV_s and, consequently, to a decrease in their G_t. Equations (7) and (8) are the simplest possible, and fundamentally explain the observed sensory effect. Many reasonable variants of other reactions between gas molecules and previously chemisorbed O^- ions on the surface of metal oxide semiconductors have been proposed.

The interaction of gas molecules with $O_2^-{}_{(c)}$ is not considered in detail in the literature. The authors in [72–74] consider that the processes of interactions of gas molecules with $O^-_{(c)}$ and $O_2^-{}_{(c)}$ are similar, but the corresponding reactions are not given. It can be assumed that there is a step-by-step interaction of gas molecules with $O_2^-{}_{(c)}$. At high operating temperatures $O_2^-{}_{(c)}$ ions are predominant and a dissociative adsorption of gas molecules occurs on the semiconductor surface. In the example of H_2, a similar process can be represented as follows:

$$\begin{gathered} H_2 \rightarrow 2H, \\ H + O_2^-{}_{(c)} \rightarrow OH^-_{(c)} + e; \\ OH^-_{(c)} \rightarrow OH + e. \end{gathered} \quad (9)$$

After the dissociation of the molecule, the atomic hydrogen H interacts with the $O_2^-{}_{(c)}$ ion, resulting in formation of a hydroxyl group $OH^-_{(c)}$ on the semiconductor surface with a localized electron, and an electron enters the TiO_2 conduction band. The $OH^-_{(c)}$ groups neutralize and desorb on the semiconductor surface [75].

4. Conclusions

The structural, electrically conductive, and gas-sensitive properties of TiO_2 films, with thicknesses of 130 nm and 463 nm, synthesized by the IBSD method, and subjected to high-temperature annealing in air were investigated. The IBSD TiO_2 films annealed at 800 °C and 1000 °C belong to the rutile phase of TiO_2. The electrically conductive properties of TiO_2 thin films in dry pure air are similar to those of bulk samples obtained by melt and high-temperature methods. The effect of H_2, CO, CO_2, NO_2, NO, CH_4 and O_2 on the electrically conductive properties of TiO_2 thin films in the operating temperature range of 200–750 °C was studied. The prospects of TiO_2 films deposited by IBSD for the development of high temperature operating O_2 sensors were demonstrated. The operating temperature of the maximum response to O_2 corresponded to 750 °C. TiO_2 films with a thickness of 130 nm and annealed at 800 °C manifested the highest response to O_2, which was 7.5 arb. un. when exposed to 40 vol. %. An increase in the annealing temperature up to 1000 °C at the same film thickness made it possible to reduce the response and recovery times by 2 times, due to changes appearing in the microstructure of the film surface. The films exhibited high responses to H_2 and NO_2 at an operating temperature of 600 °C and the largest sensitivity to nitrogen-containing oxides. An appropriate mechanism of the sensory effect in IBSD TiO_2 thin films was proposed. The great significance of various atomic forms of chemisorbed oxygen on the semiconductor surface was revealed.

Author Contributions: Conceptualization, A.V.A.; methodology, B.O.K., V.V.K., V.A.N., M.M.Z., N.N.Y. (Nikolay N. Yudin) and A.V.C.; software, V.V.K.; validation, A.V.A. and N.N.Y. (Nikita N. Yakovlev); formal analysis, A.V.A., N.N.Y. (Nikita N. Yakovlev), V.V.K. and V.A.N.; investigation, N.N.Y. (Nikita N. Yakovlev), B.O.K., V.V.K., V.A.N., M.M.Z., N.N.Y. (Nikolay N. Yudin), S.N.P., N.N.E., A.V.C. and M.P.S.; resources, M.M.Z., N.N.E. and A.S.O.; data curation, A.V.A. and N.N.Y. (Nikita N. Yakovlev); writing—original draft preparation, H.B.; writing—review and editing, A.V.A.; visualization, N.N.Y. (Nikita N. Yakovlev); supervision, A.V.A.; project administration, A.V.A.; funding acquisition, A.V.A. All authors have read and agreed to the published version of the manuscript.

Funding: The research was carried out with the support of a grant under the Decree of the Government of the Russian Federation No. 220 of 9 April 2010 (Agreement No. 075-15-2022-1132 of 1 July 2022) and Ministry of Science and Higher Education of the Russian Federation, project No. FSWM-2020-0038. Studies of the deposition of TiO_2 films by the IBS were supported by a grant from the Russian Science Foundation No. 22-22-20103 (https://rscf.ru/project/22-22-20103/ (accessed on 1 September 2022)) and funds of the Tomsk Region Administration.

Institutional Review Board Statement: Not applicable.

Informed Consent Statement: Not applicable.

Data Availability Statement: All data that support the findings of this study are included within the article.

Conflicts of Interest: The authors declare no conflict of interest.

References

1. Wang, Y.; Wu, T.; Zhou, Y.; Meng, C.; Zhu, W.; Liu, L. TiO_2-based nanoheterostructures for promoting gas sensitivity performance: Designs, developments, and prospects. *Sensors* **2017**, *17*, 1971. [CrossRef] [PubMed]
2. Tian, X.; Cui, X.; Lai, T.; Ren, J.; Yang, Z.; Xiao, M.; Wang, B.; Xiao, X.; Wang, Y. Gas sensors based on TiO_2 nanostructured materials for the detection of hazardous gases: A review. *Nano Mater. Sci.* **2021**, *3*, 390–403. [CrossRef]
3. Rzaij, J.; Abass, A. Review on: TiO_2 thin film as a metal oxide gas sensor. *J. Chem. Rev.* **2020**, *2*, 114–121. [CrossRef]
4. Larsson, H.; Yakimova, R.; Zolnai, Z.; Ivanov, I.; Monemar, B.; Gogova, D. Fast growth of high quality GaN. *Phys. Status Solidi a* **2003**, *20*, 13–17. [CrossRef]
5. Almaev, A.; Nikolaev, V.; Butenko, P.; Stepanov, S.; Pechnikov, A.; Yakovlev, N.; Sinyugin, I.; Shapenkov, S.; Scheglov, M. Gas sensors based on pseudohexagonal phase of gallium oxide. *Phys. Status Solidi b* **2021**, *259*, 2100306. [CrossRef]
6. Kachel, K.; Korytov, M.; Gogova, D.; Galazka, Z.; Albrecht, M.; Zwierz, R.; Siche, D.; Golka, S.; Kwasniewski, A.; Schmidbauer, M.; et al. A new approach to free-standing GaN using β-Ga_2O_3 as a substrate. *CrystEngComm* **2012**, *14*, 8536–8540. [CrossRef]
7. Almaev, A.V.; Yakovlev, N.N.; Chernikov, E.V.; Tolbanov, O.P. Selective sensors of nitrogen dioxide based on thin tungsten oxide films under optical irradiation. *Tech. Phys. Lett.* **2019**, *45*, 1016–1019. [CrossRef]

8. Ramanavicius, S.; Tereshchenko, A.; Karpicz, R.; Ratautaite, V.; Bubniene, U.; Maneikis, A.; Jagminas, A.; Ramanavicius, A. TiO_{2-x}/TiO_2-structure based 'self-heated' sensor for the determination of some reducing gases. *Sensors* **2020**, *20*, 74. [CrossRef]
9. Zakrzewska, K.; Radecka, M. TiO_2-based nanomaterials for gas sensing—influence of anatase and rutile contributions. *Nanoscale Res. Lett.* **2017**, *12*, 89. [CrossRef]
10. Li, Z.; Jun, Y.X.; Haidry, A.A.; Plecenik, T.; Juan, X.L.; Chao, S.L.; Fatima, Q. Resistive-type hydrogen gas sensor based on TiO_2: A review. *Int. J. Hydrogen Energy* **2018**, *43*, 21114–21132. [CrossRef]
11. Nunes, D.; Fortunato, E.; Martins, R. Flexible nanostructured TiO_2-based gas and UV sensors: A review. *Discov. Mater.* **2022**, *2*, 2. [CrossRef]
12. Li, T.; Rui, Y.; Zhang, X.; Shi, J.; Wang, X.; Wang, Y.; Yang, J.; Zhang, Q. Anatase TiO_2 nanorod arrays as high-performance electron transport layers for perovskite solar cells. *J. Alloys Compd.* **2020**, *849*, 156629. [CrossRef]
13. Illarionov, G.A.; Morozova, S.M.; Chrishtop, V.V.; Einarsrud, M.A.; Morozov, M.I. Memristive TiO_2: Synthesis, technologies, and applications. *Front. Chem.* **2020**, *8*, 724. [CrossRef] [PubMed]
14. Lin, J.; Heo, Y.U.; Nattestad, A.; Sun, Z.; Wang, L.; Kim, J.H.; Dou, Z.X. 3D hierarchical rutile TiO_2 and metal-free organic sensitizer producing dye-sensitized solar cells 8.6 % conversion efficiency. *Sci. Rep.* **2014**, *4*, 5769. [CrossRef] [PubMed]
15. He, X.; Wu, M.; Ao, Z.; Lai, B.; Zhou, Y.; An, T.; Wang, S. Metal–organic frameworks derived C/TiO_2 for visible light photocatalysis: Simple synthesis and contribution of carbon species. *J. Hazard. Mater.* **2021**, *403*, 124048. [CrossRef]
16. Ratan, S.; Kumar, C.; Kumar, A.; Kumar, D.J.; Kumar, A.M.; Kumar, R.U.; Pratap, A.S.; Jit, S. Room temperature high hydrogen gas response in $Pd/TiO_2/Si/Al$ capacitive sensor. *Micro Nano Lett.* **2020**, *15*, 632–635. [CrossRef]
17. Dwivedi, D.; Dwivedi, R.; Srivastava, S.K. The effect of hydrogen-induced interface traps on a titanium dioxide-based palladium gate MOS capacitor (Pd-MOSC): A conductance study. *Microelectron. J.* **1998**, *29*, 445–450. [CrossRef]
18. Mardare, D.; Cornei, N.; Mita, C.; Florea, D.; Stancu, A.; Tiron, V.; Manole, A.; Adomnitei, C. Low temperature TiO_2 based gas sensors for CO_2. *Ceram. Int.* **2016**, *42*, 7353–7359. [CrossRef]
19. Rydosz, A.; Brudnik, A.; Staszek, K. Metal oxide thin films prepared by magnetron sputtering technology for volatile organic compound detection in the microwave frequency range. *Materials* **2019**, *12*, 877. [CrossRef]
20. Moumen, A.; Kumarage, G.C.W.; Comini, E. P-type metal oxide semiconductor thin films: Synthesis and chemical sensor applications. *Sensors* **2022**, *22*, 1359. [CrossRef]
21. Nafarizal, N. Precise control of metal oxide thin films deposition in magnetron sputtering plasmas for high performance sensing devices fabrication. *Procedia Chem.* **2016**, *20*, 93–97. [CrossRef]
22. Chaluvadi, S.K.; Mondal, D.; Bigi, C.; Knez, D.; Rajak, P.; Ciancio, R.; Fujii, J.; Panaccione, G.; Vobornik, I.; Rossi, G.; et al. Pulsed laser deposition of oxide and metallic thin films by means of Nd:YAG laser source operating at its 1st harmonics: Recent approaches and advances. *J. Phys. Mater.* **2021**, *4*, 032001. [CrossRef]
23. Filipescu, M.; Papavlu, A.P.; Dinescu, M. Functional metal oxide thin films grown by pulsed laser deposition. In *Crystalline and Non-Crystalline Solids*; Mandracci, P., Ed.; IntechOpen: London, UK, 2016. [CrossRef]
24. Huotari, J.; Kekkonen, V.; Puustinen, J.; Liimatainen, J.; Lappalainen, J. Pulsed laser deposition for improved metal-oxide gas sensing layers. *Procedia Eng.* **2016**, *168*, 1066–1069. [CrossRef]
25. Huotari, J.; Lappalainen, J.; Puustinen, J.; Baur, T.; Alepee, C.; Haapalainen, T.; Komulainen, S.; Pylvanainen, J.; Lloyd, A.S. Pulsed laser deposition of metal oxide nanoparticles, agglomerates, and nanotrees for chemical sensors. *Procedia Eng.* **2015**, *120*, 1158–1161. [CrossRef]
26. Hamid, N.; Suhaimi, S.; Othman, M.Z.; Ismail, W.Z.W. A Review on thermal evaporation method to synthesis zinc oxide as photocatalytic material. *Nano Hybrids Compos.* **2021**, *31*, 55–63. [CrossRef]
27. Mukherjee, S. Thin film deposition from dual ion beam sputtering system. *CSI Trans. ICT* **2019**, *7*, 99–104. [CrossRef]
28. Bundesmann, C.; Neumann, H. Tutorial: The systematics of ion beam sputtering for deposition of thin films with tailored properties. *J. Appl. Phys.* **2018**, *124*, 231102. [CrossRef]
29. Bundesmann, C.; Amelal, T. Secondary particle properties for the ion beam sputtering of TiO_2 in a reactive oxygen atmosphere. *Appl. Surf. Sci.* **2019**, *485*, 391–401. [CrossRef]
30. Bundesmann, C.; Lautenschläger, T.; Spemann, D.; Finzel, A.; Thelander, E.; Mensing, M.; Frost, F. Systematic investigation of the properties of TiO_2 films grown by reactive ion beam sputter deposition. *Appl. Surf. Sci.* **2017**, *421*, 331–340. [CrossRef]
31. Bundesmann, C.; Lautenschläger, T.; Spemann, D.; Thelander, E. Reactive Ar ion beam sputter deposition of TiO_2 films: Influence of process parameters on film properties. *Nucl. Instrum. Methods Phys. Res. Sect. B Beam Interact. Mater. At.* **2017**, *395*, 17–23. [CrossRef]
32. Amelal, T.; Pietzonka, L.; Rohkamm, E.; Bundesmann, C. Properties of secondary particles for the reactive ion beam sputtering of Ti and TiO_2 using oxygen ions. *J. Vac. Sci. Technol. A* **2020**, *38*, 033403. [CrossRef]
33. Jung, H.; Min, H.; Hwang, J.; Kim, J.; Choe, Y.; Lee, H.; Lee, W. Selective detection of sub-1-ppb level isoprene using Pd-coated In_2O_3 thin film integrated in portable gas chromatography. *Appl. Surf. Sci.* **2022**, *586*, 152827. [CrossRef]
34. Kalanov, D.; Unutulmazsoy, Y.; Spemann, D.; Bauer, J.; Anders, A.; Bundesmann, C. Properties of gallium oxide thin films grown by ion beam sputter deposition at room temperature. *J. Vac. Sci. Technol. A* **2022**, *40*, 033409. [CrossRef]
35. Choe, Y. New gas sensing mechanism for SnO_2 thin-film gas sensors fabricated by using dual ion beam sputtering. *Sens. Actuators B Chem.* **2001**, *77*, 200–208. [CrossRef]

36. Min, B.K.; Choi, S.D. C_4H_{10} sensing characteristics of ion beam sputtered SnO_2 sensors. *Sens. Actuators B Chem.* **2005**, *108*, 125–129. [CrossRef]
37. Min, B.K.; Choi, S.D. SnO_2 thin film gas sensor fabricated by ion beam deposition. *Sens. Actuators B Chem.* **2004**, *98*, 239–246. [CrossRef]
38. Prasad, A.K.; Kubinski, D.J.; Gouma, P.I. Comparison of sol–gel and ion beam deposited MoO_3 thin film gas sensors for selective ammonia detection. *Sens. Actuators B Chem.* **2003**, *93*, 25–30. [CrossRef]
39. Simion, C.E.; Schipani, F.; Papadogianni, A.; Stanoiu, A.; Budde, M.; Oprea, A.; Weimar, U.; Bierwagen, O.; Barsan, N. Conductance model for single-crystalline/compact metal oxide gas-sensing layers in the nondegenerate limit: Example of epitaxial SnO_2 (101). *ACS Sens.* **2019**, *4*, 2420–2428. [CrossRef]
40. Liu, Y.; Parisi, J.; Sun, X.; Lei, Y. Solid-state gas sensors for high temperature applications—A review. *J. Mater. Chem. A* **2014**, *2*, 9919. [CrossRef]
41. Golubović, A.; Nikolić, S.; Djurić, S.; Valčić, A. The growth of sapphire single crystals. *J. Serb. Chem. Soc.* **2001**, *66*, 411–418. [CrossRef]
42. Almaev, A.V.; Kushnarev, B.O.; Chernikov, E.V.; Novikov, V.A.; Korusenko, P.M.; Nesov, S.N. Structural, electrical and gas-sensitive properties of Cr_2O_3 thin films. *Superlattices Microstruct.* **2021**, *151*, 106835. [CrossRef]
43. Qing, H.; Lian, G. A simple route for the synthesis of rutile TiO_2 nanorods. *Chem. Lett.* **2003**, *32*, 638–639. [CrossRef]
44. Wang, D.; Choi, D.; Yang, Z.; Viswanathan, V.V.; Nie, Z.; Wang, C.; Song, Y.; Zhang, J.-G.; Liu, J. Synthesis and Li-ion insertion properties of highly crystalline mesoporous rutile TiO_2. *Chem. Mater.* **2008**, *20*, 3435–3442. [CrossRef]
45. Abazović, N.D.; Čomor, M.I.; Dramićanin, M.D.; Jovanović, D.J.; Ahrenkiel, S.P.; Nedeljković, J.M. Photoluminescence of anatase and rutile TiO_2 particles. *J. Phys. Chem. B* **2006**, *110*, 25366–25370. [CrossRef] [PubMed]
46. Miao, L.; Jin, P.; Kaneko, K.; Terai, A.; Nabatova-Gabain, N.; Tanemura, S. Preparation and characterization of polycrystalline anatase and rutile TiO_2 thin films by rf magnetron sputtering. *Appl. Surf. Sci.* **2003**, *212–213*, 255–263. [CrossRef]
47. Haidry, A.A.; Schlosser, P.; Durina, P.; Mikula, M.; Tomasek, M.; Plecenik, T.; Roch, T.; Pidik, A.; Stefecka, M.; Noskovic, J.; et al. Hydrogen gas sensors based on nanocrystalline TiO_2 thin films. *Cent. Eur. J. Phys.* **2011**, *9*, 1351. [CrossRef]
48. Nadzirah, S.; Hashim, U.; Kashif, M.; Shamsuddin, S.A. Stable electrical, morphological and optical properties of titanium dioxide nanoparticles affected by annealing temperature. *Microsyst. Technol.* **2017**, *23*, 1743–1750. [CrossRef]
49. Soussi, A.; Ait Hssi, A.; Boujnah, M.; Boulkadat, L.; Abouabassi, K.; Asbayou, A.; Elfanaoui, A.; Markazi, R.; Ihlal, A.; Bouabid, K. Electronic and optical properties of TiO_2 thin films: Combined experimental and theoretical study. *J. Electron. Mater.* **2021**, *50*, 4497–4510. [CrossRef]
50. Korotcenkov, G.; Brinzari, V.; Golovanov, V.; Blinov, Y. Kinetics of gas response to reducing gases of SnO_2 films, deposited by spray pyrolysis. *Sens. Actuators B Chem.* **2004**, *98*, 41–45. [CrossRef]
51. Weibel, A.; Bouchet, R.; Knauth, P. Electrical properties and defect chemistry of anatase (TiO_2). *Solid State Ion.* **2006**, *177*, 229–236. [CrossRef]
52. Nowotny, M.K.; Bak, T.; Nowotny, J. Electrical properties and defect chemistry of TiO_2 single crystal. I. Electrical conductivity. *J. Phys. Chem. B* **2006**, *110*, 16270–16282. [CrossRef] [PubMed]
53. Gan, L.; Wu, C.; Tan, Y.; Chi, B.; Pu, J.; Jian, L. Oxygen sensing performance of Nb-doped TiO_2 thin film with porous structure. *J. Alloy. Compd.* **2014**, *585*, 729–733. [CrossRef]
54. Li, M.; Chen, Y. An investigation of response time of TiO_2 thin-film oxygen sensors. *Sens. Actuators B Chem.* **1996**, *32*, 83–85. [CrossRef]
55. Kirner, U.; Schierbaum, K.D.; Göpel, W.; Leibold, B.; Nicoloso, N.; Weppner, W.; Fischer, D.; Chu, W.F. Low and high temperature TiO_2 oxygen sensors. *Sens. Actuators B Chem.* **1990**, *1*, 103–107. [CrossRef]
56. Bartic, M.; Toyoda, Y.; Baban, C.; Ogita, M. Oxygen sensitivity in gallium oxide thin films and single crystals at high temperatures. *Jpn. J. Appl. Phys.* **2006**, *45*, 5186. [CrossRef]
57. Maksimova, N.K.; Almaev, A.V.; Sevastyanov, E.Y.; Potekaev, A.I.; Chernikov, E.V.; Sergeychenko, N.V.; Korusenko, P.M.; Nesov, S.N. Effect of additives Ag and rare-earth elements Y and Sc on the properties of hydrogen sensors based on thin SnO_2 films during long-term testing. *Coatings* **2019**, *9*, 423. [CrossRef]
58. Lu, C.; Huang, Y.; Huang, J.; Chang, C.; Wu, S. A Macroporous TiO_2 oxygen sensor fabricated using anodic aluminium oxide as an etching mask. *Sensors* **2010**, *10*, 670–683. [CrossRef]
59. Wang, Y.; Lai, X.; Liu, B.; Chen, Y.; Lu, Y.; Wang, F.; Zhang, L. UV-induced desorption of oxygen at the TiO_2 surface for highly sensitive room temperature O_2 sensing. *J. Alloy. Compd.* **2019**, *793*, 583–589. [CrossRef]
60. Haidry, A.A.; Xie, L.; Wang, Z.; Zavabeti, A.; Li, Z.; Plecenik, T.; Gregor, M.; Roch, T.; Plecenik, A. Remarkable improvement in hydrogen sensing characteristics with Pt/TiO_2 interface control. *ACS Sens.* **2019**, *4*, 2997–3006. [CrossRef]
61. Kumar, M.; Singh Bhati, V.; Kumar, M. Effect of Schottky barrier height on hydrogen gas sensitivity of metal/TiO_2 nanoplates. *Int. J. Hydrog. Energy* **2017**, *42*, 22082–22089. [CrossRef]
62. Arifin, P.; Mustajab, M.A.; Haryono, S.; Adhika, D.R.; Nugraha, A.A. MOCVD growth and characterization of TiO_2 thin films for hydrogen gas sensor application. *Mater. Res. Express* **2019**, *6*, 076313. [CrossRef]
63. Lu, C.; Chen, Z. High-temperature resistive hydrogen sensor based on thin nanoporous rutile TiO_2 film on anodic aluminum oxide. *Sens. Actuators B Chem.* **2009**, *140*, 109–115. [CrossRef]

64. Samransuksamer, B.; Jutarosaga, T.; Horprathum, M.; Wisitsoraat, A.; Eiamchai, P.; Limwichean, S.; Patthanasettakul, V.; Chananonnawathorn, C.; Chindaudom, P. Highly sensitive H_2 sensors based on Pd- and PdO-decorated TiO_2 thin films at low-temperature operation. *Key Eng. Mater.* **2016**, *675–676*, 277–280. [CrossRef]
65. Xie, T.; Sullivan, N.; Steffens, K.; Wen, B.; Liu, G.; Debnath, R.; Davydov, A.; Gomez, R.; Motayed, A. UV-assisted room-temperature chemiresistive NO_2 sensor based on TiO_2 thin film. *J. Alloy. Compd.* **2015**, *653*, 255–259. [CrossRef] [PubMed]
66. Boyadjiev, S.; Georgieva, V.; Vergov, L.; Baji, Z.; Gáber, F.; Szilágyi, I.M. Gas sensing properties of very thin TiO_2 films prepared by atomic layer deposition (ALD). *J. Phys. Conf. Ser.* **2014**, *559*, 012013. [CrossRef]
67. Rumyantseva, M.N.; Makeeva, E.A.; Gaskov, A.M. Influence of the microstructure of semiconductor sensor materials on oxygen chemisorption on their surface. *Russ. J. Gen. Chem.* **2008**, *78*, 2556–2565. [CrossRef]
68. Almaev, A.V.; Chernikov, E.V.; Novikov, V.V.; Kushnarev, B.O.; Yakovlev, N.N.; Chuprakova, E.V.; Oleinik, V.L.; Lozinskaya, A.D.; Gogova, D.S. Impact of Cr_2O_3 additives on the gas-sensitive properties of β-Ga_2O_3 thin films to oxygen, hydrogen, carbon monoxide, and toluene vapors. *J. Vac. Sci. Technol. A* **2021**, *39*, 023405. [CrossRef]
69. Saruhan, B.; Fomekong, L.R.; Nahirniak, S. Review: Influences of semiconductor metal oxide properties on gas sensing characteristics. *Front. Sens.* **2021**, *2*, 657931. [CrossRef]
70. Badalyan, S.M.; Rumyantseva, M.N.; Smirnov, V.V.; Alikhanyan, A.S.; Gaskov, A.M. Effect of Au and NiO catalysts on the NO_2 sensing properties of nanocrystalline SnO_2. *Inorg. Mater.* **2010**, *46*, 232–236. [CrossRef]
71. Gautam, Y.K.; Sharma, K.; Tyagi, S.; Ambedkar, A.K.; Chaudhary, M. Nanostructured metal oxide semiconductor-based sensors for greenhouse gas detection: Progress and challenges. *R. Soc. Open Sci.* **2021**, *8*, 201324. [CrossRef]
72. Jiménez-Cadena, G.; Riu, J.; Rius, F.X. Gas sensors based on nanostructured materials. *Analyst* **2007**, *132*, 1083–1099. [CrossRef]
73. Yamazoe, N.; Fuchigami, J.; Kishikawa, M.; Seiyama, T. Interactions of tin oxide surface with O_2, H_2O and H_2. *Surf. Sci.* **1979**, *86*, 335–344. [CrossRef]
74. Yamazoe, N.; Sakai, G.; Shimanoe, K. Oxide semiconductor gas sensors. *Catal. Surv. Asia* **2003**, *7*, 63–75. [CrossRef]
75. Gaman, V.I.; Almaev, A.V. Dependences of characteristics of sensors based on tin dioxide on the hydrogen concentration and humidity of gas mixture. *Russ. Phys. J.* **2017**, *60*, 90–100. [CrossRef]